

Magnetic dichroism in $L_{2,3}$ emission of Fe, Co, and Ni following energy-dependent excitation with circularly polarized x rays

L.-C. Duda

Department of Physics, Box 530, Uppsala University, S-751 21 Uppsala, Sweden

J. Stöhr

IBM Research Division, Almaden Research Center, 650 Harry Road, San Jose, California 95120

D. C. Mancini, A. Nilsson, N. Wassdahl, and J. Nordgren

Department of Physics, Box 530, Uppsala University, S-751 21 Uppsala, Sweden

M. G. Samant

IBM Research Division, Almaden Research Center, 650 Harry Road, San Jose, California 95120

(Received 21 July 1994)

The magnetic dichroism in the $L_{2,3}$ emission spectra of Fe, Co, and Ni, following excitation with circularly polarized x rays, is found to exhibit a dramatic dependence on excitation energy. The observed changes in sign and intensity of the dichroism spectra are explained by a simple model and are shown to negate the use of x-ray fluorescence yield detection for quantitative dichroism absorption measurements. Multielectron effects are found to be minimized by use of monochromatic threshold excitation.

X-ray magnetic circular dichroism (XMCD) spectroscopy is based on the differential absorption cross section of left and right circularly polarized x rays in magnetic materials.¹ In the past, XMCD studies have typically been carried out by measuring x-ray *absorption* (XA) which through core-to-valence transitions monitors the element-specific, local magnetic properties of the unoccupied valence bands. The measured XA dichroism intensities are directly linked through sum rules^{2,3} to the spin- and angular-momentum-dependent hole population of the valence shell in the ground state, i.e., to the local spin and orbital moments. Besides element-specific moments, it is also of great interest to know the element-specific energy-dependent spin-distribution in the valence shell. It has recently been proposed theoretically⁴ and shown experimentally⁵ that the spin-dependent density of occupied states can be obtained from a valence-to-core x-ray *emission* (XE) spectrum, following the creation of a spin polarized core hole through absorption of circularly polarized x rays. The XE dichroism spectrum is the difference in emission intensity obtained with opposite relative orientations of the photon spin (helicity) of the incident x rays and magnetization direction of the sample.

Here we demonstrate the importance of using energy-selective excitation for XE dichroism spectroscopy. While theoretically proposed,⁴ such experiments have been impeded by insufficient photon flux. For this reason, the only previous XE dichroism measurement⁵ used broad bandpass (white light) circular polarized x rays for the excitation process. Our experiments demonstrate the importance of creating a well-defined core hole state by using monochromatic threshold excitation. At higher excitation energies, we observe strong multielectron and Coster-Kronig satellites which complicate the interpretation of the XE spectrum. We also observe a strong excitation energy dependence of the XE dichroism intensity which is explained in a simple model.

These results demonstrate that the XE dichroism intensity is not directly proportional to the XA dichroism signal. This is a demonstration of the breakdown of an important experimental concept, namely the use of fluorescence detection as a measure of x-ray absorption.

The experiments were carried out on beam line 8-2 at the Stanford Synchrotron Radiation Laboratory (SSRL). The 90% circularly polarized x rays from the storage ring⁶ were monochromatized with a spherical grating monochromator (1100 l/mm grating) to an energy width of ~ 4 eV. At 50 mA storage ring current the flux on the sample was about 1×10^{12} photons/sec. The samples consisted of 400-Å-thick films of Fe, Co, and Ni, protected by a 50-Å-thick Cu capping layer, grown by dc sputtering on a silicon wafer substrate. All films had an in-plane easy axis of magnetization and saturation fields of < 25 Oe. The samples were positioned in the gap between two solenoids inside a vacuum chamber. The magnetic field of 28 Oe was parallel to the incident x rays, which were incident on the sample at a 20° angle from the surface. The field direction was reversed every 60 sec to minimize artifacts due to current decay or small storage ring instabilities, and a computer acquired and added the data for each direction separately. The x-ray emission spectrometer consisted of an entrance slit, three spherical diffraction gratings, and a two-dimensional position-sensitive multichannel detector.⁷ It was oriented with its optical axis perpendicular to the incident x rays, in a vertically dispersive geometry and was operated with a 1200 l/mm grating in second order at a spectral resolution of 3 eV. Typical count rates were about 20 counts/sec in the L_3 emission peak.

For brevity, we shall mainly discuss the XE spectra of Co metal below. Results for Ni and Fe will be presented in tabular form only. X-ray emission spectra were recorded at four excitation energies, illustrated in Fig. 1(a) for the XA dichro-

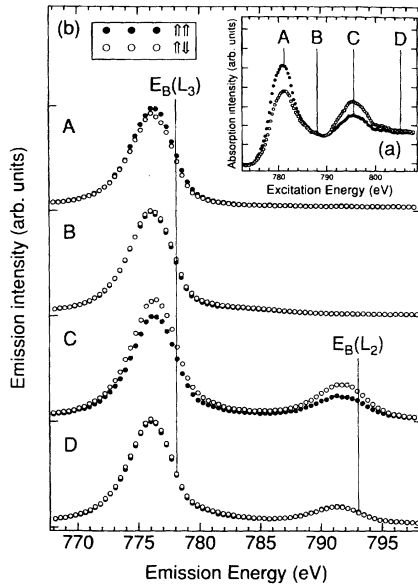


FIG. 1. (a) X-ray absorption dichroism spectrum of a 400-Å Co film, recorded by total electron yield detection, with parallel (filled circles) and antiparallel (open circles) alignment of photon spin and sample magnetization directions, respectively. The same energy resolution as for the x-ray emission spectra shown in (b) was used. (b) Co $L_{2,3}$ XE spectra for the same 400-Å Co film, excited with parallel (filled circles) and antiparallel (open circles) alignment of photon spin and sample magnetization directions, at excitation energies (A)–(D), indicated in (a). The Co $2p_{3/2}$ and $2p_{1/2}$ binding energies relative to the Fermi level are indicated as $E_B(L_3)$ and $E_B(L_2)$, respectively.

ism spectrum of Co: (A) on the L_3 resonance, (B) between the L_3 and L_2 resonances, (C) on the L_2 resonance, and (D) above the L_2 resonance. The corresponding XE spectra of Co metal for the two alignments of photon spin and magnetization direction are shown in Fig. 1(b).

The XE dichroism spectra for Co, i.e. the difference spectra of those shown in Fig. 1(b), are shown in Fig. 2(a). The dichroism intensity is given in percent of the L_3 peak height in the original spectra. We have also indicated by a vertical line the Co $2p_{3/2}$ and $2p_{1/2}$ binding energies $E_B(L_3)$ and $E_B(L_2)$,⁹ corresponding to the L_3 and L_2 excitation thresholds. There are three striking effects in the dichroism spectra: (1) the change of sign of the intensity with excitation energy, (2) the giant dichroism effect following L_2 resonance excitation, and (3) the significant dichroism intensity above $E_B(L_3)$, between the L_3 and L_2 emission peaks, in cases B–D.

For the context of the present paper we shall restrict our discussion to the thin-sample limit, where a direct comparison can be made between the dichroism effects measured in XA and XE. The thin-limit spectra were obtained by use of energy-dependent correction functions⁸ derived from high-resolution XMCD absorption spectra of the metals, scaled in the pre- and post-edge regions to tabulated absorption coefficients.¹⁰ The XA and XE energy scales were aligned by using literature values for the Fe, Co, and Ni $2p_{3/2}$ binding energies⁹ and the L_3 emission energies.¹¹ The dichroism XE spectra of Co, corrected for the thin limit, are shown in Fig. 2(b).

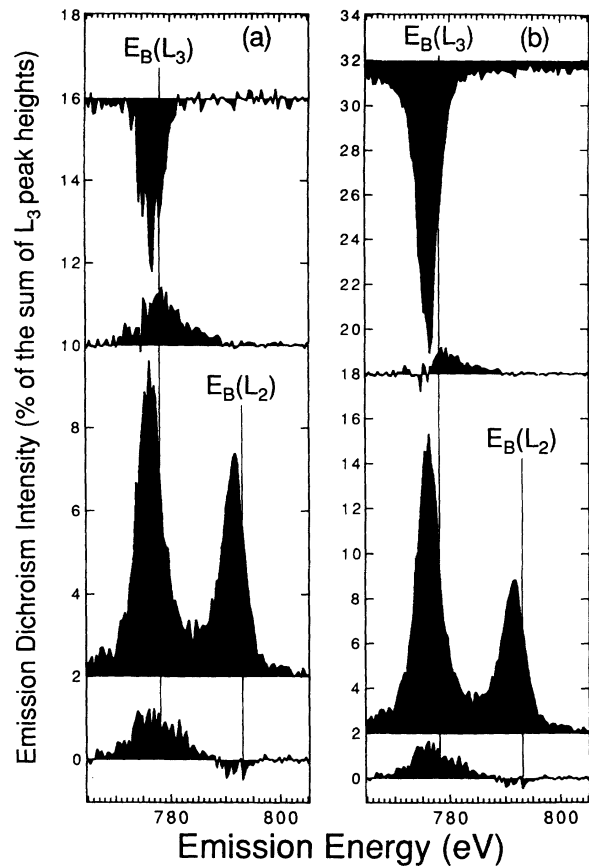


FIG. 2. (a) Difference spectra of the XE spectra shown in Fig. 1(b) (antiparallel minus parallel alignments) for cases A–D, from top to bottom, respectively. (b) Difference spectra corrected for the thin-sample limit, as discussed in the text. Spectra are vertically offset for clarity.

The strong energy dependence in the thin limit can be understood in a simple one-electron rigid-band model, illustrated in Fig. 3. For the XA process we assume dipole transitions for right and left circularly polarized x rays from the $2p_j$ ($j=3/2, 1/2$) core level to the spin-split d band,¹² and describe the XE process by spin-conserving dipole transitions summed over all x-ray polarizations. We denote the total number of spin-up and spin-down empty d states as N_{\uparrow}^e and N_{\downarrow}^e and filled d states as N_{\uparrow}^f and N_{\downarrow}^f , so that the magnetic spin moment is given by $\mu_S = (N_{\uparrow}^e - N_{\downarrow}^e)\mu_B = (N_{\uparrow}^f - N_{\downarrow}^f)\mu_B$. In this model the integrated XA dichroism intensity, associated with L_3 and L_2 resonance excitation, is given by¹²

$$\Delta I_j^{XA} = A(1-j)[N_{\downarrow}^e - N_{\uparrow}^e]\alpha(1-j)\mu_S, \quad (1)$$

where the constant A is proportional to a squared dipole matrix element, and the factor $(1-j)$ leads to a change in sign of the XA dichroism intensity at the L_3 and L_2 edges. If we ignore Coster-Kronig decay, the XE dichroism intensity, defined as the difference of the XE intensities measured with right and left circularly polarized excitation, is given by

$$\Delta I_j^{XE} = B(1-j)[N_{\downarrow}^e \tilde{N}_{\downarrow}^f - N_{\uparrow}^e \tilde{N}_{\uparrow}^f], \quad (2)$$

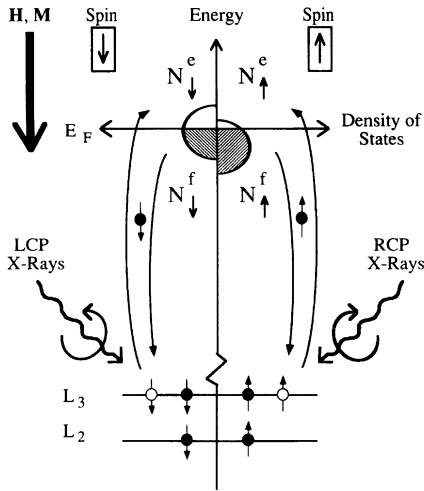


FIG. 3. One-electron model used to explain the XE dichroism process and intensities. The d band is split into spin-up and spin-down bands, and the number of empty and filled bands is denoted as N^e and N^f , respectively. The absorption of right and left circularly polarized x rays by the spin-orbit split $2p$ shell creates spin-polarized core holes of opposite spin orientation. These holes are filled by spin-conserving dipole transitions from the spin-split d band. We assume that the polarization of the emitted fluorescent x rays is not analyzed. The arrow marked **H**, **M** denotes the direction of the external magnetic field **H** and the sample magnetization **M**.

where the constant B is the product of squared excitation and deexcitation dipole matrix elements, and N^f is the number of filled d states on the excited atom in the presence of a core hole in the $2p$ shell. In general, the presence of the core hole will decrease the number of empty and increase the number of filled d states on the excited atom, similar to the case of a $Z+1$ impurity atom in a host of atoms with atomic number Z . According to the initial- and final-state rules,^{12,13} the presence of the core hole influences the x-ray emission intensity but not the integrated x-ray absorption intensity. For simplicity, we shall neglect the core hole effect in the following discussion, i.e., we shall assume $N^f = N^f$.

The sign of the observed XE dichroism intensity in the thin limit, shown in Fig. 2(b), is readily explained by Eq. (2). For *resonant* excitation at the L_3 or L_2 edges we can rewrite Eq. (2) as

$$\Delta I_j^{\text{XE}} \propto (1-j)[N_{\downarrow}^f - N_{\uparrow}^e] \mu_S \propto [N_{\downarrow}^f - N_{\uparrow}^e] \Delta I_j^{\text{XA}}, \quad (3)$$

and since $N_{\downarrow}^f - N_{\uparrow}^e$ is positive for Co metal,¹⁴ the XE and XA dichroic signals have the same sign. For *nonresonant* excitation, i.e., above the L_3 or L_2 resonances, the photoelectron is excited into states well above the Fermi level and to a good approximation $N_{\downarrow}^e = N_{\uparrow}^e$, such that the XA dichroism intensity is zero [Eq. (1)]. The XE dichroism intensity [Eq. (2)] takes the form

$$\Delta I_j^{\text{XE}} \propto -(1-j) \mu_S \quad (4)$$

and the XE dichroism changes sign. This case also illustrates the inequivalence of the XA and XE dichroism effects, since the XE dichroism is finite while the XA dichroism vanishes.

The anomalously large dichroism intensity for resonant L_2 -edge excitation, seen in Figs. 1(b) and 2, is explained by

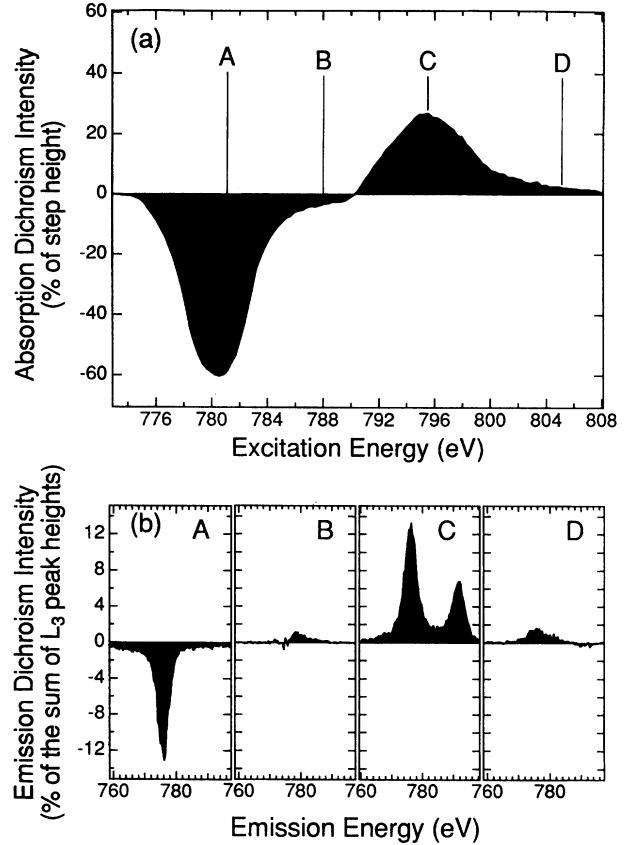


FIG. 4. (a) XA dichroism spectrum of Co corresponding to the difference of the spectra in Fig. 1(a). (b) XE dichroism spectra of Co obtained at the excitation energies A–D indicated in (a).

the presence of spin-orbit effects (orbital moment) in the d band. In a one-electron model appropriate for a d^9 electronic configuration,¹² the spin-orbit interaction splits the d band into “less-filled” $d_{5/2}$ and “more-filled” $d_{3/2}$ components. Since $p_{1/2} \leftrightarrow d_{5/2}$ transitions are dipole forbidden, the L_2 -edge XA dichroism intensity is reduced relative to the L_3 intensity.^{2,6} In contrast, the L_2 XE intensity is enhanced since the term $N_{\downarrow}^f - N_{\uparrow}^e$ in Eq. (3) becomes effectively larger. For L_2 resonant excitation, the spin-orbit interaction can be viewed as effectively reducing the available number of empty states and increasing the available number of filled states. The spectra in Fig. 2(b) show that for resonant L_2 excitation the L_3 emission dichroism intensity is also enhanced. This can be explained by Coster-Kronig decay. The fact that the L_3 and L_2 intensities have the same sign indicates spin conservation in the Coster-Kronig process.

Figure 4 shows that the observed XE dichroism intensities do not quantitatively follow the XA dichroism intensities, measured at the same excitation energies A–D. Note, for example, that the XA and XE dichroism intensities for excitation energy B exhibit opposite sign. Also the absolute value of the XA dichroism intensity for resonant L_3 excitation (A) is larger than that for resonant L_2 excitation (C), while the reverse is true for the XE intensities.

Similar observations hold for the XA and XE dichroism effects for Fe and Ni which are summarized in Table I together with those for Co. In order to directly compare the XA

TABLE I. $L_{3,2}$ XA and XE dichroism intensity ratios $(I_A - I_P)/(I_A + I_P)$ for Fe, Co, and Ni, where I_P and I_A refer to parallel and antiparallel alignment of photon spin and sample magnetization directions, respectively. The excitation energies A–D are identified in Fig. 1(a) for Co, and are defined analogously for Fe and Ni.

	Excitation energy (eV)	Absorption intensity	Emission intensity
Fe	A (709)	-0.100	-0.060
	B (715)	0.014	0.050
	C (722)	0.080	0.082
	D (736)	0.012	0.024
Co	A (781)	-0.148	-0.128
	B (788)	-0.004	0.012
	C (796)	0.121	0.159
	D (805)	0.015	0.018
Ni	A (855)	-0.064	-0.058
	B (861)	-0.021	-0.009
	C (872)	0.038	0.059
	D (887)	0.003	0.006

and XE effects we have listed the self-normalized intensity ratios $(I_A - I_P)/(I_A + I_P)$, where the subscripts refer to parallel and antiparallel alignment of photon spin and sample magnetization directions, respectively. Comparison of the intensity ratios listed in Table I clearly demonstrate the inequivalence of the absorption and emission intensities. The most important result is the reversal of the relative dichroism intensities at the L_3 and L_2 resonance energies (A and C in Table I). In XA the L_3 dichroism intensity is larger than the L_2 intensity while the reverse holds for XE. This fact is due to the spin-orbit interaction in the d band, as discussed above, and it has an important consequence. Since the relative size of the L_3 and L_2 dichroism intensities measured in XA are quantitatively related to the orbital magnetic moment of the d shell,² use of fluorescence detection for dichroism absorption measurements would give incorrect orbital moments.

The above results constitute a demonstration of the breakdown of using x-ray fluorescence detection as a quantitative measure of x-ray absorption. Fluorescence yield detection has been extensively used for conventional XA spectroscopy of dilute systems.¹⁵ For the study of magnetic materials, it promised the elimination of magnetic-field problems that plague electron yield detection studies.¹⁶ Since the fluorescence deexcitation channel is a minority channel (0.8%), as compared to the dominant Auger channel (99.2%),¹⁷ a significant dichroic intensity difference in the XE channel (e.g., factor of 2) will result in only a minor dichroic intensity difference in the majority Auger channel (e.g., 1% change). Electron yield detection will therefore still be a good measure of the polarization-dependent x-ray absorption coefficient.

Figure 2 reveals that, independent of how the data are treated, there is a significant dichroism intensity above the L_3 threshold at 778.1 eV, except for resonant L_3 excitation, case (A). This intensity arises from multielectron effects, i.e., multielectron-excited intermediate states and, at higher energies, Coster-Kronig decay. For threshold excitation, case A, there is only enough energy available to excite the core electron just above the Fermi level, and in this case the XE spectra have a predominantly one-electron character and are related to the electronic ground state.

Our studies point the way for future XE dichroism studies. The availability of increased circularly polarized photon flux from insertion devices will allow such experiments to be performed with highly monochromatic incident radiation, to minimize multielectron effects, and high spectral resolution in the emission channel. Such studies promise to reveal the detailed element-specific, spin-dependent density of states for complex magnetic materials and buried layers and interfaces.

We would like to thank V. Speriosu and S. Parkin for providing the Fe, Co, and Ni samples. The work was carried out in part at SSRL, which is operated by DOE, Division of Chemical Sciences. This work was supported by the Swedish Natural Science Research Council.

¹G. Schütz *et al.*, Phys. Rev. Lett. **58**, 737 (1987); C. T. Chen *et al.*, Phys. Rev. B **42**, 7262 (1990).

²B. T. Thole *et al.*, Phys. Rev. Lett. **68**, 1943 (1992).

³P. Carra *et al.*, Phys. Rev. Lett. **70**, 694 (1993).

⁴P. Strange *et al.*, Phys. Rev. Lett. **67**, 3590 (1991).

⁵C. F. Hague *et al.*, Phys. Rev. B **48**, 3560 (1993).

⁶Y. Wu *et al.*, Phys. Rev. Lett. **69**, 2307 (1992).

⁷J. Nordgren *et al.*, Rev. Sci. Instrum. **60**, 1690 (1989).

⁸*Principles of Quantitative X-Ray Fluorescence Analysis*, edited by R. Tertian and F. Claisse (Heyden and Sons, London, 1982).

⁹J. Fuggle and N. Mårtensson, J. Electron Spectrosc. Relat. Phenom. **21**, 275 (1980). We assumed that the inflection point at the low-energy side of the L_3 absorption peak coincides with the $2p_{3/2}$ binding energy.

¹⁰B. L. Henke *et al.*, At. Data Nucl. Data Tables **27**, 1 (1982).

¹¹J. A. Bearden and A. F. Burr, Rev. Mod. Phys. **39**, 125 (1967).

¹²J. Stöhr and Y. Wu, in *New Directions in Research with 3rd Generation Soft X-Ray Synchrotron Radiation Sources*, Nato ASI Series E, Vol 254, edited by A. S. Schlachter and F. J. Wuilleumier (Kluwer Academic, Dordrecht, Netherlands, 1994), p. 221.

¹³A. F. Starace, Phys. Rev. B **5**, 1773 (1972); V. I. Grebennikov *et al.*, Phys. Status Solidi B **79**, 423 (1977); **80**, 73 (1977); E. O. F. Zdansky *et al.*, Phys. Rev. B **48**, 2632 (1993).

¹⁴D. A. Papaconstantopoulos, *Handbook of the Band Structure of Elemental Solids* (Plenum, New York, 1986).

¹⁵See, for example, *X-Ray Absorption, Principles, Applications, Techniques of EXAFS, SEXAFS, and XANES*, edited by D. C. Koningsberger and R. Prins (Wiley, New York, 1988).

¹⁶C. T. Chen *et al.*, Phys. Rev. B **48**, 642 (1993).

¹⁷M. O. Krause, J. Phys. Chem. Ref. Data **8**, 307 (1979).